

# 國立交通大學

工學院精密與自動化工程學程

## 碩士論文

以循圓測試法建立 HexGlider 型平行機構之運動誤差模型  
與診斷方法

Modeling and Diagnosis of Motion Error of a HexGlider  
Manipulator Based on a Circular Test Method



研究生：陳裕都  
指導教授：成維華 博士

中華民國 九十五年 七月

以循圓測試法建立 HexGlider 型平行機構之運動誤差模型與診斷  
方法

Modeling and Diagnosis of Motion Error of a HexGlider Manipulator  
Based on a Circular Test Method

研究生：陳裕都  
指導教授：成維華 博士

Student : Yu-Du Chen  
Advisor : Dr. Wei-Hua Chieng

國立交通大學

工學院精密與自動化工程學程



Submitted to Degree Program of Automation and Precision Engineering

College of Engineering  
National Chiao Tung University  
in Partial Fulfillment of the Requirements  
for the Degree of  
Master of Science

In  
Automation and Precision Engineering  
July 2006  
Hsinchu, Taiwan, Republic of China

中華民國 九十五年 七月

# 以循圓測試法建立 HexGlider 型平行機構之運動誤差模型與 診斷方法

學生：陳裕都

指導教授：成維華 博士

國立交通大學精密與自動化工程學程碩士班

## 摘 要

本論文主要研究的範疇與目的，係針對 Hexglider 構型之平行機構的運動誤差，建立其數學模型與診斷方法。

首先，對於所欲研究之平行機構，建立其導致運動誤差的幾何誤差源模型。除了推導該種構型平行機構的驅動滑塊與輸出平台之間運動轉換的關係，同時分析出可能導致其發生運動誤差的幾何誤差源與相關之參數誤差，並利用於運動轉換關係所得到的結果，建構個別誤差源之誤差模型，以瞭解各誤差源在理論上對於該機構之運動精度所造成的影響。

更進一步，以實驗的方式，對此待測之平行機構，進行實機之雙球桿循圓測試，來作誤差診斷。其主要目標，在於找出該機構可能存在之幾何誤差源，並且診斷各誤差源之參數誤差的大小。

在數學上，本論文將利用最小平方法原理，將整個平行機構綜合誤差經循圓測試所量得軌跡，解構為由個別誤差源所對應之循圓運動軌跡的合成，並將針對個別誤差之參數誤差進行估測，以實現該機構之誤差診斷，適當地發展出該機構運動誤差的校驗方法。換言之，只要運用雙球桿量測裝置，正確地對待測之平行機構，量得循圓運動軌跡，即可有效地分析出該機構之各項幾何誤差源，並且診斷其誤差參數之大小。如此，不論是對於該種平行機構之機械本體的精度的改善，或者是終端輸出的位置誤差的補償，都將會有莫大的助益。

# **Modeling and Diagnosis of Motion Error of a HexGlider Manipulator Based on a Circular Test Method**

Student : Yu-Du Chen

Advisors : Dr. Wei-Hua Chieng

Institute of Automation and Precision Engineering  
National Chiao Tung University

## **Abstract**

This thesis is mainly focused on the study of analyzing and identifying specified motion errors for the hexglider type of parallel manipulator.

First, the investigated geometric errors resulting in motion errors for the target parallel manipulator are to be modeled. We begin at deriving the kinematic transformation relationships between the sliders and the end effector of the parallel manipulator. Geometric resources of motional deviations, including translate and angular ones, resulting from the manufacturing or assembly of guideways and linkages are classified and modeled with the analytical results of the kinematics.

Next, the double ball bar test is experimentally applied to the desired parallel manipulator for the study of the error diagnosis. We aim to identify geometric errors existing at the manipulator from the measured data.

Mathematically, the least square method is adopted in the thesis to the identification of geometric errors. The circular contour of the overall error of the parallel mechanism obtained from the double ball bar test will be fitted by theoretic deviations caused by error sources, and their parameter errors are to be estimated.

Based on the results, we will propose a measurement method and evaluating procedure to identify geometric deviations. It can be utilized as a calibration method of the hexglider manipulator. In other words, provided that the double ball bar test is applied to the desired parallel manipulator correctly, geometric deviations existing at the manipulator can be identified. Thus, it will significantly benefit to either the compensation of the position and orientation errors or the improvement of the mechanism accuracy for the hexglider type of parallel manipulator.

## 誌 謝

本論文之完成，首先要感謝指導教授 成維華博士，在我碩士班的求學期間，諄諄教誨，循循善誘，不論是在理論或實驗上，皆不厭其煩地給予諸多的指導與啟發，令我在學問的追求與學理的研究上，除了累積豐富的知識與難得的經驗，同時也獲得相當程度的成長。

感謝所有口試委員深刻且獨到的指教，由於您們寶貴的意見，使得本論文更具可讀性。

在出社會工作多年之後，選擇重回學校讀書研究，父母的認同與支持，給了我極大的勇氣與信心；他們多年來無微不至的教養與提攜，黑髮換白髮，成就了今日的我。謹以獲得此一學位的榮耀，獻給最摯愛的雙親。

特別感謝博士班游武璋學長關於機構誤差理論的推導，楊家豐學長在最小平方法應用上的討論，還有童永成學長與吳炳霖同學在實驗上的鼎力協助，同時也要感謝交通大學機研所智慧機電實驗室提供模擬器平台。有了大家的幫忙，克服了每個過程中所遭遇的種種困難，使得整個論文的研究工作，得以順利地完成。

最後，對於所有家人以及關心我的友人，由衷地感謝您們在這段日子裏，持續不斷地對我的關懷與鼓勵。

# Contents

摘要	i
Abstract	ii
誌謝	iii
Content	iv
List of Figures	vi
List of Tables	viii
<b>Chapter 1 Introduction</b>	<b>1</b>
1.1 Parallel manipulator	1
1.2 Motion Errors	2
1.3 Literature Review	4
<b>Chapter 2 Kinematics Transformation</b>	<b>10</b>
2.1 SP-120 Hexglider Manipulator	10
2.2 Inverse Kinematics	11
2.3 Kinematics of RSSR Mechanisms	16
2.4 Newton-Raphson Method	17
2.5 Forward Kinematics	21
<b>Chapter 3 Modeling of Motion Errors</b>	<b>24</b>
3.1 Introduction	24
3.2 Error Descriptions	24
3.3 Error Modeling	26
3.4 Error Diagnosis	35
<b>Chapter 4 Measurement of Motion Errors</b>	<b>37</b>
4.1 Double Ball Bar Measurement Device	37
4.2 Experimental Planning	38

4.3	Experimental Results	39
<b>Chapter 5</b>	<b>Least Squares Estimation</b>	41
5.1	Error Estimation	41
5.2	Least Square Method	42
5.3	Simulation and Diagnosis	44
5.4	Discussion	45
<b>Chapter 6</b>	<b>Conclusion</b>	48
<b>Reference</b>		49



## **List of Figures**

Figure 1.1	Outline of this Study	53
Figure 1.2	Prototype of SP-120	54
Figure 2.1	Hexglider parallel manipulator	55
Figure 2.2	Geometric relationships with respect to the mobile plate and the fixed plate	55
Figure 2.3	Geometric relationships with respect to the two linkages and two sliders on a guideway	56
Figure 2.4	RSSR mechanism	56
Figure 2.5	Forward kinematics of the hexglider manipulator under investigation	57
Figure 3.1	Geometric error sources of a hexglider manipulator	57
Figure 3.2 (a)	Guideway translation error	58
Figure 3.2 (b)	Guideway rotation error I	58
Figure 3.2 (c)	Guideway rotation error II	58
Figure 3.3	Guideway translation error along X-axis for RSSR mechanism__Type I	59
Figure 3.4	Guideway translation error along X-axis for RSSR mechanism__Type II	59
Figure 3.5	Guideway translation error along Y-axis for RSSR mechanism__Type I	60
Figure 3.6	Guideway translation error along Y-axis for RSSR mechanism_Type II	60
Figure 3.7	Guideway translation error along Z-axis for RSSR Mechanism__Type I	61
Figure 3.8	Guideway translation error along Z-axis for RSSR Mechanism__Type II	61
Figure 3.9	Guide way rotation error on XY plane for RSSR	62



	mechanism_Type I	
Figure 3.10	Guide way rotation error on XY plane for RSSR	62
	mechanism_Type II	
Figure 3.11	Guide way rotation error on YZ plane for RSSR	63
	mechanism_Type I	
Figure 3.12	Guide way rotation error on YZ plane for RSSR	63
	mechanism_Type II	
Figure 3.13	Guide way rotation error about the center of the base for RSSR mechanism_Type I	64
Figure 3.14	Guide way rotation error about the center of the base for RSSR mechanism_Type II	64
Figure 3.15	Procedures of modeling the overall profile error	65
Figure 3.16	Error simulation (1)_linkage length error ( $\delta=0.01\text{mm}$ )	66
Figure 3.17	Error simulation (2)_slides positioning error ( $\delta=0.01\text{mm}$ )	67
Figure 3.18	Error simulation (3)_guideway assembly error ( $\delta=0.01\text{mm}$ )	68
Figure 3.19	Error simulation (4)_guideway rotation error ( $\varepsilon=0.01\text{deg}$ )	69
Figure 3.20	Error simulation (5)_guideway rotation error ( $\varepsilon=0.01\text{deg}$ )	70
Figure 4.1	Configuration of the error diagnosis experiment	71
Figure 4.2	Double ball bar system	72
Figure 4.3	Procedures of DBB test & error diagnosis	73
Figure 4.4	Procedures of the setup and data capture of the DBB test	74
Figure 4.5	Design of the auxiliary fixture for DBB test	75
Figure 4.6	Testing path of the circular contour tracking	75
Figure 4.7	The completed setup of the DBB system	76
Figure 4.8	Polar plot obtained from the data capture of DBB test	76
Figure 5.1	Procedures of curve fitting with least square estimation	77
Figure 5.2	Polar plot of error estimation	78

## **List of Table**

Table 1.1	Resources of motion errors	79
Table 3.1	Parameter errors corresponding to the geometric errors for a hexglider manipulator	80
Table 3.2	Characteristic equations of geometric errors for the RSSR mechanism	81
Table 3.3	Systems of error equations for the parall hexglider manipulator	82
Table 5.1	Error estimation with given errors (1)	83
Table 5.2	Error estimation with given errors (2)	83
Table 5.3	Error estimation with given errors (3)	84
Table 5.4	Error estimation with given errors (4)	84
Table 5.5	Error estimation with given errors (5)	85
Table 5.6	Error estimation with given errors (6)	85
Table 5.7	Error estimation with given errors (7)	86
Table 5.8	Error estimation with data based on DBB test for the manipulator SP-120	86

# Chapter 1

## Introduction

### §1-1 Parallel Manipulator

Parallel manipulators have recently attracted increasing attentions for many applications. Numerous researchs and development efforts were devoted on them. It is well known that most industrial robots are open-chain mechanisms constructed of consecutive links connected by rotational or prismatic one degree of freedom. These serial manipulators have large workspace, high dexterity and good maneuverability. However, they exhibit low stiffness and poor positioning accuracy due to their serial structure. As a result, their applications that require large load (e.g. machining) and high accuracy are limited.

The parallel manipulator, the end effector is attached to a movable plate which is supported in-parallel by a number of actuated links, is anticipated to possess the following advantages compared with serial manipulators : 1) High force / torque capacity since the load is distributed to several in-parallel actuators ; 2) High structural rigidity ; and 3) Better accuracy due to less cumulative joint errors.

For the high accuracy motion control of the parallel kinematic feed drive system, it is crucial to accurately calibrate various errors of kinematic parameters such as the reference length of the strut or the location of the slide

joint. In practice, the knowledge of these identified errors is beneficial to improving the position and orientation accuracy of a parallel manipulator.

In our study, we will develop a diagnostic method for identifying kinematic parameter errors based on the DBB test, which have been widely accepted by machine tool manufactures as a standard tool to measure the contouring accuracy and diagnose error sources for conventional multi-axis machine tools. Figure 1.1 outlines the main structure of this thesis. A hexglider type of parallel manipulator developed by the intelligent mech-electric labroatory in NCTU, named SP-120 as shown in Figure 1.2, is utilized as an experimental manipulator throughout this study.



## §1-2 Motion Errors

Motion errors are defined as the difference between the real and measured position and orientation of the end effector. These errors cause a deterioration of the machine performace, which in turn directly influences the final product specifications. In order to maintain high quality of performace, these errors have to be detected and eliminated.

The kinematic precision is an important item to evaulate the performance of a machine / manipulator. From the point view of kinematic precision, it means that the precision in position, velocity, and acceleration of a machine

during normal operations[1]. For a drive system with ball screws and guideways, the manufacturing error of the machine parts, the feed motion error, and the command error may have a fatal influence on the point-to-point precision of the machining workpiece or the contouring precision of the end-effector.

One of the significant requirements for the kinematic precision is to generate the movement in different axes of a machine so that the end effector can position and orientate precisely. The contouring precision of the end-effector, a kind of the positional precision, is the accuracy of the overall system or the contour error of the system. This is defined as the actual difference in distance between the programmed path and the actual path. The contouring error is the synthetic performance of several kinds of error sources. For a machine with the drive systems of ball screws and guideways, error sources can be categorized into groups such as the position error, the feed motion error, and the command error, as illustrated in Table 1.1.[2]

Geometric errors of a manipulator are resulted from not only the manufacturing process but also the improper assembly. They include the length error of the linkage, the elastic deformation of each guideway, and the symmetric angular and positional errors of the guideways. Compared with the other errors, geometric errors are more stable and controlled easier.

Sp-120 is a parallel manipulator with the drive systems of ball screws and guideways. The improper assembly of guideways fixed on the stationary plate will have a great influence on the incorrect pose (position and orientation) of the end effector. Thus, the present study for the errors of the parallel manipulator will focus on modeling and identifying geometric errors, such as the reference length error of the strut, the location error of the slide joint, or the angular and positional deviations of guideways for the hexglider type of parallel manipulator.

### §1-3 Literature Review



It is very important for manufacturing a high precise machine to evaluate its performances, such as accuracy, functions, ..., etc. In view of evaluating the accuracy of a machine, proper measuring tools and correct diagnostic methods are indispensable.

Measuring tools can retrieve useful calibrating data to be analyzed from a manipulator. To evaluate a machine, one must first determine what errors to be identified so as to select a suitable measuring tool. Nowadays, there are a few measuring tools available for measuring motional errors. Coordinate Measurement Machines (CMM) can detect the spatial coordinate location of a selected contact point. Laser interferometers is ideal for measuring straightness and point-to point precision. The double ball bar (DBB) measurement systems

[3] specified in ISO 230-1 [4] as a measuring instrument has been mainly used for the circular motion tests of the conventional 3-axis machining center, and the instrument has contributed to the performance test or periodic maintenance of the machining center.

To identify errors is the major goal of implementing measurement. Two approaches, direct error identification method and indirect error identification method, are normally applied to the error identification.

The direct error identification method is performed by measuring the individual error sources directly. For example, the laser interferometer, for a translational slide, can measure six motional errors associated with a prismatic joint at different positions of moving axes of the machine in one measurement.

The indirect error identification method is the way to realize the errors of the machine by means of measuring the errors of a part profile or the overall errors of machines. Mou, Donmez and Centikunt [5] used a feature-based comparison method to correlate the dimensional and form errors of a manufactured part. Inverse kinematic methods and statistical methods were applied to estimate the contribution of the individual error component to imperfect part features.

The Double ball bar (DBB) test is another significant example. In this method, the kinematic error of the circular interpolation of a machine is read by using a LVDT scale, and then is transmitted to a computer to be processed further. Based on the error models and the principles of statistics, not only

individual errors existing at the mechanism can be identified, but what proportion of the overall noncircularity error which can be attributed to the identified error can be estimated as well.

In addition, the DBB is frequently used to measure the dynamic errors such as gain mismatch, lost motion and stick-slip. All possible error sources of NC machine tools, for example, based on the motion error contour can be diagnosed.

Bryan [6] proposed that the double ball bar (DBB) measurement system is an error diagnosis method for measuring geometric errors and dynamic characteristics. Knapp [7] studied on the relationship between the contouring error and the motion error sources. Kunzman [8] and Kakino [9] described motion errors based on DBB with the characteristic matrix and the error vector respectively. S.L.Jeng et al. [10] presented a linear model (1st order approximation) and a nonlinear model (2nd order approximation) to describe the motion error due to a faulty guide way system for the multi-axis machine. M.Tsutsumi et al. [11] presented an algorithm for identifying particular deviations such as angular deviations around linear axes relating to rotary axes in 5-axis machining center based on the DBB method.

Many publications dealt with the kinematics of Stewart platform-based manipulators have appeared since the Stewart platform was proposed by Stewart in 1965 [12]. In [13], the kinematic behavior of a three-link, three degree-of-freedom (DOF) platform was investigated. In [14], the kinematic behavior of a 6-DOF Stewart platform was studied.



The forward kinematic problem of the parallel manipulator involves systems of highly non-linear equations. Many of these studies was established on the basis of a simplified structure to reduce the nonlinearity of the equations, such that an analytical approach can be performed to complete a solution set. Important results are presented in [15] proving that the solution for spatial structures of the 3-3 type is a polynomial equation of the 16<sup>th</sup> degree, while the solution in case of 6-6 system is a polynomial equation of the 40<sup>th</sup> order [16] (there may exist up to 64 solutions which make this an impossible approach to use practically.). There also exist numerical methods that can be used to compute all of the forward kinematic solutions of parallel manipulators that have a more general configurations. These methods relied on the numerical continuation method or exhaustive mono-dimensional-search algorithm to solve the polynomial form of the loop closure equations[17 ][18 ].

Several papers discussed the accuracy analysis of a parallel manipulator and developed error models. Wang and Masory [19] investigated how manufacturing errors affect the accuracy of a Stewart platform. Ropponen and Arai [20] presented an error model based on differentiation of the kinematics. Wang and Ehmman [21] developed error models for the Stewart platform using differential leg length changes. K.C.Fan et al. [22] dealt with the verification of two error modeling methods, namely linkage kinematic error analysis method and the differential vector method, for the parallel machine tool structure. Although each model follows slightly different formulation, they are all able to

take errors in kinematic errors and calculate the resulting pose error. Some also calculate error sensitivities and present automated error analysis simulations.

A few authors have also presented calibration algorithms for the Stewart platform. Zhuang and Roth [23] developed a calibration method that holds one leg length fixed while varying the others, allowing the kinematic parameters of each leg to be identified individually while redundant parameters are limited. Wampler et al. [24] developed a slightly different type of calibration based on implicit loops. A method to use redundant sensors on passive joints to calibrate parallel manipulators was formulated by Zhuang and Liu [25]. K.F.Ehmann et al. [26] presented a calibration method using a ball bar or other simple length measuring device to act as an ‘extra leg’ for the calibration of kinematic parameters of the hexapod. M.H.Perng et al. [27] presents a novel self-calibration strategy for a general hexapod manipulator using trigger probe and a cylindrical gauge block. The algorithm is formulated to solve a nonlinear least squares problem that takes all measurement errors into account.

This thesis is organized into six chapters. The first chapter serves as a brief introduction. Chapter 2 presents the kinematic models of the hexglider parallel manipulator including the inverse kinematic and forward kinematic equations. Chapter 3 constructs a variety of models of the circular contouring deviations resulting from geometric errors. Chapter 4 contains the descriptions of the device, setup, and procedure applied to the experiment in the study. Chapter 5 presents the error estimation based on the least square technique. Chapter 6

concludes the work by presenting the achievements, and indicating the areas remaining for the further study.



## Chapter 2

### Kinematics Transformations

## §2-1 SP-120 Hexglider Parallel Manipulator

SP-120 is a six degrees-of-freedom (DOF) hexglider type of parallel mechanism. It mainly consists of an upper mobile plate, a lower stationary plate, six motors, and six linkages, as shown in Figure 1.2. Each of the six linkages connects to a slider with one end and links to the mobile plate with the other end. Six AC servomotors driving sliders through couplings and ball screws can move linkages indirectly. The working principle of the manipulator is that the controller accepts external signals or commands and outputs motion commands to servomotors for moving linkages. With displacements of linkages, the end-effector can be translated and orientated properly. Any set of the spatial position and posture of the end-effector may correspond to a set of positions of sliders. The geometric configuration of the manipulator affects the mobility of the end-effector. The length of the linkage, the travel distance of the slider, and the rotating range of the joint can not only limit the workspace of the end-effector but affect the output velocity of the actuator.

In comparison with the serial mechanism, SP-120 may have better accuracy due to the excellent rigidity resulting from dispersing loads to multiple linkages and the less accumulated errors. However, the workspace of

SP-120 is obviously smaller than the serial mechanism. This disadvantage should be taken into account and evaluated properly while applying such manipulator for industry.

## §2-2 Inverse Kinematics

Figure 2.1 shows a type of hexglider parallel manipulator. The centers of the ball joints on the mobile plate are denoted as  $Q_1$ ,  $Q_2$ , and  $Q_3$ .  $Q_1 Q_2 Q_3$  is an equilateral-triangle with each side of a length  $a$ .  $B_1 B_2 B_3$  is an equilateral-triangle on the fixed lower plate with each side of a length  $b$ .  $S_1 \sim S_6$  specify the positions of six sliders. Each of the six linkages, with a length  $l$ , is linked to the movable upper plate through a ball joint. The other ends of them are connected with a slider travelling on the guideway mounted on the lower fixed plate by a universal joint. Figure 2.2 shows the definitions of geometric relationships existing at the movable plate and the fixed plate. From the results of the geometric relationship, the coordinates of  $B_1$ ,  $B_2$ , and  $B_3$  of the fixed plate with respect to the base frame are :

$$X_{B_1} = \frac{\sqrt{3}}{6}b \quad , \quad X_{B_2} = \frac{\sqrt{3}}{6}b \quad , \quad X_{B_3} = -\frac{\sqrt{3}}{3}b$$

$$Y_{B_1} = -\frac{b}{2} \quad , \quad Y_{B_2} = \frac{b}{2} \quad , \quad Y_{B_3} = 0$$

$$Z_{B_1} = 0 \quad , \quad Z_{B_2} = 0 \quad , \quad Z_{B_3} = 0$$

The coordinates of  $Q_1, Q_2, Q_3$  of the movable plate with respect to the top frame are :

$$x_{Q1} = \frac{\sqrt{3}}{3} a \quad , \quad x_{Q2} = -\frac{\sqrt{3}}{6} a \quad , \quad x_{Q3} = -\frac{\sqrt{3}}{6} a$$

$$y_{Q1} = 0 \quad , \quad y_{Q2} = \frac{a}{2} \quad , \quad y_{Q3} = -\frac{a}{2}$$

$$z_{Q1} = 0 \quad , \quad z_{Q2} = 0 \quad , \quad z_{Q3} = 0$$

The homogeneous transformation from the top to the base frames is described by the transformation matrix :

$$[T_{Base}^{Top}] = \begin{bmatrix} \cos \beta \cos \gamma & \sin \alpha \sin \beta \cos \gamma & \cos \alpha \sin \beta \sin \gamma & P_X \\ \cos \alpha \sin \gamma & \sin \alpha \sin \beta \sin \gamma + \cos \alpha \cos \gamma & \cos \alpha \sin \beta \sin \gamma - \sin \alpha \cos \gamma & P_Y \\ -\sin \beta & \sin \alpha \cos \beta & \cos \alpha \cos \beta & P_Z \\ 0 & 0 & 0 & 1 \end{bmatrix}$$

$$= \begin{bmatrix} u_X & v_X & w_X & P_X \\ u_Y & v_Y & w_Y & P_Y \\ u_Z & v_Z & w_Z & P_Z \\ 0 & 0 & 0 & 1 \end{bmatrix} \quad (2.1)$$

The coordinates of the origin of the top frame with respect to the base frame are denoted by  $[P_X \cdot P_Y \cdot P_Z]^T$ . Let  $\alpha, \beta, \gamma$  represent the rotation angles defined by rotating the top frame first about the X axis with  $\alpha$  degrees, then about the Y axis with  $\beta$  degrees, and finally about the Z axis with  $\gamma$  degrees, respectively. The coordinates of  $Q_i, i=1, 2, 3$ , in terms of the base frame can be calculated through

$$\begin{bmatrix} X_{Q_i} \\ Y_{Q_i} \\ Z_{Q_i} \\ 1 \end{bmatrix} = [T_{Base}^{Top}](P_X, P_Y, P_Z, \alpha, \beta, \gamma) \begin{bmatrix} x_{Q_i} \\ y_{Q_i} \\ z_{Q_i} \\ 1 \end{bmatrix}, \quad i = 1 \sim 3 \quad (2.2)$$

Consequently, the coordinates of  $Q_1$ ,  $Q_2$ , and  $Q_3$  with respect to the base frame can be computed

$$\begin{aligned} & \begin{bmatrix} X_{Q1} \\ Y_{Q1} \\ Z_{Q1} \\ 1 \end{bmatrix} \\ &= [T_{Base}^{Top}] \begin{bmatrix} x_{Q1} \\ y_{Q1} \\ z_{Q1} \\ 1 \end{bmatrix} \\ &= \begin{bmatrix} u_x & v_x & w_x & P_X \\ u_y & v_y & w_y & P_Y \\ u_z & v_z & w_z & P_Z \\ 0 & 0 & 0 & 1 \end{bmatrix} \begin{bmatrix} \sqrt{3}a \\ 3 \\ 0 \\ 0 \\ 1 \end{bmatrix} \end{aligned} \quad \begin{aligned} & \text{ES} \\ & 1896 \end{aligned}$$

$$= \begin{bmatrix} P_X + \frac{\sqrt{3}a}{3}u_x \\ P_Y + \frac{\sqrt{3}a}{3}u_y \\ P_Z - \frac{\sqrt{3}a}{3}u_z \\ 1 \end{bmatrix} \quad (2.3)$$

$$\begin{aligned}
 & \begin{bmatrix} X_{Q2} \\ Y_{Q2} \\ Z_{Q2} \\ 1 \end{bmatrix} \\
 &= [T_{Base}^{Top}] \begin{bmatrix} x_{Q2} \\ y_{Q2} \\ z_{Q2} \\ 1 \end{bmatrix} \\
 &= \begin{bmatrix} u_x & v_x & w_x & P_x \\ u_y & v_y & w_y & P_y \\ u_z & v_z & w_z & P_z \\ 0 & 0 & 0 & 1 \end{bmatrix} \begin{bmatrix} -\frac{\sqrt{3}a}{6} \\ \frac{a}{2} \\ 0 \\ 1 \end{bmatrix}
 \end{aligned}$$

$$= \begin{bmatrix} P_x - \frac{\sqrt{3}a}{6}u_x + \frac{a}{2}v_x \\ P_y - \frac{\sqrt{3}a}{6}u_y + \frac{a}{2}v_y \\ P_z - \frac{\sqrt{3}a}{6}u_z + \frac{a}{2}v_z \\ 1 \end{bmatrix}$$



(2.4)

$$\begin{aligned}
 & \begin{bmatrix} X_{Q3} \\ Y_{Q3} \\ Z_{Q3} \\ 1 \end{bmatrix} \\
 &= [T_{Base}^{Top}] \begin{bmatrix} x_{Q3} \\ y_{Q3} \\ z_{Q3} \\ 1 \end{bmatrix}
 \end{aligned}$$



$$\begin{aligned}
&= \begin{bmatrix} u_x & v_x & w_x & P_X \\ u_y & v_y & w_y & P_Y \\ u_z & v_z & w_z & P_Z \\ 0 & 0 & 0 & 1 \end{bmatrix} \begin{bmatrix} \frac{\sqrt{3}a}{6} \\ -\frac{a}{2} \\ 0 \\ 1 \end{bmatrix} \\
&= \begin{bmatrix} P_X - \frac{\sqrt{3}a}{6}u_x - \frac{a}{2}v_x \\ P_Y - \frac{\sqrt{3}a}{6}u_y - \frac{a}{2}v_y \\ P_Z - \frac{\sqrt{3}a}{6}u_z - \frac{a}{2}v_z \\ 1 \end{bmatrix} \tag{2.5}
\end{aligned}$$

Figure 2.3 illustrates a ball joint has two adjacent equal-length linkages connected to two sliders movable on one of the three guideways mounted on the stationary plate.  $Q_i$  is the ball joint.  $S_{2i-1}$  and  $S_{2i}$  are linear sliders. The length of  $B_{2i} B_{2i-1}$  is  $b$ .  $Q_i F_{2i-1}$  and  $Q_i F_{2i}$  are the linkages with a length  $l$ .

Then

$$\begin{aligned}
t_{2i}^2 &= t_{2i-1}^2 + b^2 - 2t_{2i-1}b \cos \varphi_i, \quad i = 1 \sim 3 \\
\varphi_i &= \cos^{-1} \left[ \frac{t_{2i-1}^2 - t_{2i}^2 + b^2}{2t_{i-1}b} \right] \tag{2.6}
\end{aligned}$$

$$l^2 = t_{2i-1}^2 + \hat{S}_{2i-1}^2 - 2t_{2i-1}\hat{S}_{2i-1} \cos \varphi_i,$$

the distance between  $B_{2i}$  and  $S_{2i-1}$  yields

$$\hat{S}_{2i-1} = t_{2i-1} \cos \varphi_i - \sqrt{l^2 - t_{2i-1}^2 \sin^2 \varphi_i}, \quad i = 1 \sim 3 \tag{2.7}$$

$$l^2 = t_{2i-1}^2 + (b - \hat{S}_{2i})^2 - 2t_{2i-1}(b - \hat{S}_{2i}) \cos \varphi_i,$$

the distance between  $B_{2i-1}$  and  $S_{2i}$  yields

$$\hat{S}_{2i} = (b - t_1 \cos \varphi_i) - \sqrt{l^2 - t_{2i-1}^2 \sin^2 \varphi_i}, \quad i = 1 \sim 3 \quad (2.8)$$

### §2-3 Kinematics of RSSR Mechanisms

The conventional forward kinematics for the six degree-of-freedom manipulator needs complicated mathematic operations. The forward kinematic problem involves systems of highly non-linear equations. Many of these studies was established on the basis of a simplified structure to reduce the nonlinearity of the equations, such that an analytical approach can be performed to complete the solution set.

The proposed forward kinematics used in this chapter needs at first to decomposite the hexglider parallel manipulator into three sets of RSSR structures. After deriving the kinematic relationships existing at the RSSR mechanism mounting on any guideway of the hexglider parallel manipulator, we can intergrate all of the three ones and solve the simultaneous equations to describe the behavior of the hexglider manipulator.

As shown in Figure 2.4, the positions of the ball joints U1 and U2 can be expressed as follows:

$$U1 = Trans(0, -f, 0) \cdot Rot(y, -\theta) \begin{bmatrix} 0 \\ 0 \\ r \end{bmatrix} \quad (2.9)$$

$$U2 = Rot(z, -60^\circ) \cdot Trans(0, -g, 0) \cdot Rot(y, \delta) \begin{bmatrix} 0 \\ 0 \\ q \end{bmatrix} \quad (2.10)$$

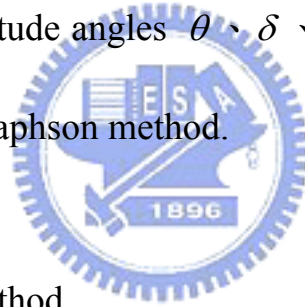
The distance between U1 and U2 yields

$$\begin{aligned} b^2 &= f^2 + g^2 + q^2 + r^2 - fg - 2qr\sin(\delta)\sin(\theta) \\ &- \sqrt{3}fq\sin(\delta) - \sqrt{3}gr\sin(\theta) + qr\sin(\delta)\sin(\theta) \end{aligned} \quad (2.11)$$

Eq (2.11) can be expressed as follows

$$\begin{aligned} F^* &= f^2 + g^2 + q^2 + r^2 - b^2 - fg - 2qr\sin(\delta)\sin(\theta) \\ &- \sqrt{3}fq\sin(\delta) - \sqrt{3}gr\sin(\theta) + qr\sin(\delta)\sin(\theta) \end{aligned} \quad (2.12)$$

Thus, the approximate attitude angles  $\theta$  ,  $\delta$  ,  $\phi$  , as shown in Fig 2.5, can be computed by Newton-Raphson method.



## §2-4 Newton-Raphson Method

Consider a system of equations 
$$\begin{cases} F_1(\theta, \delta, \phi) = 0 \\ F_2(\theta, \delta, \phi) = 0 \\ F_3(\theta, \delta, \phi) = 0 \end{cases}$$
 . Using the Taylor series

expansion with respect to  $F_1(\theta, \delta, \phi), F_2(\theta, \delta, \phi), F_3(\theta, \delta, \phi)$  about the current point

$X_0(\theta_0, \delta_0, \phi_0)$  and neglecting terms of order two and higher, we obtain

$$\begin{cases} -F_1(\theta_0, \delta_0, \phi_0) \approx \frac{\partial F_1(\theta_0, \delta_0, \phi_0)}{\partial \theta}(\theta - \theta_0) + \frac{\partial F_1(\theta_0, \delta_0, \phi_0)}{\partial \delta}(\delta - \delta_0) + \frac{\partial F_1(\theta_0, \delta_0, \phi_0)}{\partial \phi}(\phi - \phi_0) \\ -F_2(\theta_0, \delta_0, \phi_0) \approx \frac{\partial F_2(\theta_0, \delta_0, \phi_0)}{\partial \theta}(\theta - \theta_0) + \frac{\partial F_2(\theta_0, \delta_0, \phi_0)}{\partial \delta}(\delta - \delta_0) + \frac{\partial F_2(\theta_0, \delta_0, \phi_0)}{\partial \phi}(\phi - \phi_0) \\ -F_3(\theta_0, \delta_0, \phi_0) \approx \frac{\partial F_3(\theta_0, \delta_0, \phi_0)}{\partial \theta}(\theta - \theta_0) + \frac{\partial F_3(\theta_0, \delta_0, \phi_0)}{\partial \delta}(\delta - \delta_0) + \frac{\partial F_3(\theta_0, \delta_0, \phi_0)}{\partial \phi}(\phi - \phi_0) \end{cases}$$

(2.13)

As described above, a system of equations is given by

$$\begin{cases} F_1(\theta, \delta, \phi) = 0 \\ F_2(\theta, \delta, \phi) = 0 \\ F_3(\theta, \delta, \phi) = 0 \end{cases}$$

Applying the Taylor series expansions of  $F_1(\theta, \delta, \phi)$ ,  $F_2(\theta, \delta, \phi)$ ,  $F_3(\theta, \delta, \phi)$  about the point  $X_i(\theta_i, \delta_i, \phi_i)$  and letting  $(\theta, \delta, \phi) = (\theta_{i+1}, \delta_{i+1}, \phi_{i+1})$ , we obtain

$$\begin{cases} -F_1(\theta_i, \delta_i, \phi_i) = \frac{\partial F_1(\theta_i, \delta_i, \phi_i)}{\partial \theta}(\theta_{i+1} - \theta_i) + \frac{\partial F_1(\theta_i, \delta_i, \phi_i)}{\partial \delta}(\delta_{i+1} - \delta_i) + \frac{\partial F_1(\theta_i, \delta_i, \phi_i)}{\partial \phi}(\phi_{i+1} - \phi_i) \\ -F_2(\theta_i, \delta_i, \phi_i) = \frac{\partial F_2(\theta_i, \delta_i, \phi_i)}{\partial \theta}(\theta_{i+1} - \theta_i) + \frac{\partial F_2(\theta_i, \delta_i, \phi_i)}{\partial \delta}(\delta_{i+1} - \delta_i) + \frac{\partial F_2(\theta_i, \delta_i, \phi_i)}{\partial \phi}(\phi_{i+1} - \phi_i) \\ -F_3(\theta_i, \delta_i, \phi_i) = \frac{\partial F_3(\theta_i, \delta_i, \phi_i)}{\partial \theta}(\theta_{i+1} - \theta_i) + \frac{\partial F_3(\theta_i, \delta_i, \phi_i)}{\partial \delta}(\delta_{i+1} - \delta_i) + \frac{\partial F_3(\theta_i, \delta_i, \phi_i)}{\partial \phi}(\phi_{i+1} - \phi_i) \end{cases}$$

(2.14)

The system of equations in this study is given by

$$\begin{cases} F_1(\theta_i, \delta_i, \phi_i) = F_1(\theta_i, \delta_i) = 0 \\ F_2(\theta_i, \delta_i, \phi_i) = F_1(\delta_i, \phi_i) = 0 \\ F_3(\theta_i, \delta_i, \phi_i) = F_1(\phi_i, \theta_i) = 0 \end{cases} \quad (2.15)$$

To differential  $F_1(\theta, \delta, \phi)$ ,  $F_2(\theta, \delta, \phi)$ ,  $F_3(\theta, \delta, \phi)$  with respect to  $\phi$ ,  $\theta$ ,  $\delta$  yields

$$\frac{\partial F_1(\theta_i, \delta_i, \phi_i)}{\partial \phi} = \frac{\partial F_1(\theta_i, \delta_i)}{\partial \phi} = 0$$

$$\frac{\partial F_2(\theta_i, \delta_i, \phi_i)}{\partial \theta} = \frac{\partial F_2(\delta_i, \phi_i)}{\partial \theta} = 0$$

$$\frac{\partial F_3(\theta_i, \delta_i, \phi_i)}{\partial \delta} = \frac{\partial F_3(\phi_i, \theta_i)}{\partial \delta} = 0$$

Thus, the system of equations becomes

$$\begin{cases} -F_1(\theta_i, \delta_i, \phi_i) = -F_1(\theta_i, \delta_i) = \frac{\partial F_1(\theta_i, \delta_i)}{\partial \theta} (\theta_{i+1} - \theta_i) + \frac{\partial F_1(\theta_i, \delta_i)}{\partial \delta} (\delta_{i+1} - \delta_i) \\ -F_2(\theta_i, \delta_i, \phi_i) = -F_2(\delta_i, \phi_i) = \frac{\partial F_2(\delta_i, \phi_i)}{\partial \delta} (\delta_{i+1} - \delta_i) + \frac{\partial F_2(\delta_i, \phi_i)}{\partial \phi} (\phi_{i+1} - \phi_i) \\ -F_3(\theta_i, \delta_i, \phi_i) = -F_3(\theta_i, \phi_i) = \frac{\partial F_3(\theta_i, \phi_i)}{\partial \theta} (\phi_{i+1} - \phi_i) + \frac{\partial F_3(\theta_i, \phi_i)}{\partial \phi} (\theta_{i+1} - \theta_i) \end{cases} \quad (2.16)$$

The determinant D is presently equal to the Jacobian matrix of  $F_1(\theta, \delta, \phi)$ ,

$F_2(\theta, \delta, \phi)$ ,  $F_3(\theta, \delta, \phi)$  and denoted by

$$\begin{aligned} D &= \begin{vmatrix} \frac{\partial F_1(\theta_i, \delta_i, \phi_i)}{\partial \theta} & \frac{\partial F_1(\theta_i, \delta_i, \phi_i)}{\partial \delta} & \frac{\partial F_1(\theta_i, \delta_i, \phi_i)}{\partial \phi} \\ \frac{\partial F_2(\theta_i, \delta_i, \phi_i)}{\partial \theta} & \frac{\partial F_2(\theta_i, \delta_i, \phi_i)}{\partial \delta} & \frac{\partial F_2(\theta_i, \delta_i, \phi_i)}{\partial \phi} \\ \frac{\partial F_3(\theta_i, \delta_i, \phi_i)}{\partial \theta} & \frac{\partial F_3(\theta_i, \delta_i, \phi_i)}{\partial \delta} & \frac{\partial F_3(\theta_i, \delta_i, \phi_i)}{\partial \phi} \end{vmatrix} \\ &= \begin{vmatrix} \frac{\partial F_1(\theta_i, \delta_i)}{\partial \theta} & \frac{\partial F_1(\theta_i, \delta_i)}{\partial \delta} & 0 \\ 0 & \frac{\partial F_2(\delta_i, \phi_i)}{\partial \delta} & \frac{\partial F_2(\delta_i, \phi_i)}{\partial \phi} \\ \frac{\partial F_3(\phi_i, \theta_i)}{\partial \theta} & 0 & \frac{\partial F_3(\phi_i, \theta_i)}{\partial \phi} \end{vmatrix} \\ &= \frac{\partial F_1(\theta_i, \delta_i)}{\partial \theta} \frac{\partial F_2(\delta_i, \phi_i)}{\partial \delta} \frac{\partial F_3(\phi_i, \theta_i)}{\partial \phi} + \frac{\partial F_1(\theta_i, \delta_i)}{\partial \delta} \frac{\partial F_2(\delta_i, \phi_i)}{\partial \phi} \frac{\partial F_3(\phi_i, \theta_i)}{\partial \theta} \end{aligned} \quad (2.17)$$

To apply Cramer's rule, we can obtain the solutions of the above linear

system of equations  $\Delta\theta_i$ ,  $\Delta\delta_i$ ,  $\Delta\phi_i$  as follows

$$\begin{aligned} \Delta\theta_i &= \theta_{i+1} - \theta_i \\ &= \frac{\begin{vmatrix} -F_1(\theta_i, \delta_i) & \frac{\partial F_1(\theta_i, \delta_i)}{\partial \delta} & 0 \\ -F_2(\delta_i, \phi_i) & \frac{\partial F_2(\delta_i, \phi_i)}{\partial \delta} & \frac{\partial F_2(\delta_i, \phi_i)}{\partial \phi} \\ -F_3(\phi_i, \theta_i) & 0 & \frac{\partial F_3(\phi_i, \theta_i)}{\partial \phi} \end{vmatrix}}{D} \end{aligned}$$

$$\begin{aligned}
& -F_1(\theta_i, \delta_i) \frac{\partial F_2(\delta_i, \phi_i)}{\partial \delta} \frac{\partial F_3(\phi_i, \theta_i)}{\partial \phi} - F_3(\phi_i, \theta_i) \frac{\partial F_1(\theta_i, \delta_i)}{\partial \delta} \frac{\partial F_2(\delta_i, \phi_i)}{\partial \phi} + F_2(\delta_i, \phi_i) \frac{\partial F_1(\theta_i, \delta_i)}{\partial \delta} \frac{\partial F_3(\phi_i, \theta_i)}{\partial \phi} \\
= & \frac{\frac{\partial F_1(\theta_i, \delta_i)}{\partial \theta} \frac{\partial F_2(\delta_i, \phi_i)}{\partial \delta} \frac{\partial F_3(\phi_i, \theta_i)}{\partial \phi} + \frac{\partial F_1(\theta_i, \delta_i)}{\partial \delta} \frac{\partial F_2(\delta_i, \phi_i)}{\partial \phi} \frac{\partial F_3(\phi_i, \theta_i)}{\partial \theta}}{\frac{\partial F_1(\theta_i, \delta_i)}{\partial \theta} \frac{\partial F_2(\delta_i, \phi_i)}{\partial \delta} \frac{\partial F_3(\phi_i, \theta_i)}{\partial \phi} + \frac{\partial F_1(\theta_i, \delta_i)}{\partial \delta} \frac{\partial F_2(\delta_i, \phi_i)}{\partial \phi} \frac{\partial F_3(\phi_i, \theta_i)}{\partial \theta}}
\end{aligned} \tag{2.18}$$

$$\begin{aligned}
& \Delta \delta_i \\
= & \delta_{i+1} - \delta_i \\
= & \frac{\begin{vmatrix} \frac{\partial F_1(\theta_i, \delta_i)}{\partial \theta} & -F_1(\theta_i, \delta_i) & 0 \\ 0 & -F_2(\delta_i, \phi_i) & \frac{\partial F_2(\delta_i, \phi_i)}{\partial \phi} \\ \frac{\partial F_3(\phi_i, \theta_i)}{\partial \theta} & -F_3(\phi_i, \theta_i) & \frac{\partial F_3(\phi_i, \theta_i)}{\partial \phi} \end{vmatrix}}{D} \\
= & \frac{-F_2(\delta_i, \phi_i) \frac{\partial F_3(\phi_i, \theta_i)}{\partial \phi} \frac{\partial F_1(\theta_i, \delta_i)}{\partial \theta} - F_1(\theta_i, \delta_i) \frac{\partial F_2(\delta_i, \phi_i)}{\partial \phi} \frac{\partial F_3(\phi_i, \theta_i)}{\partial \theta} + F_3(\phi_i, \theta_i) \frac{\partial F_2(\delta_i, \phi_i)}{\partial \phi} \frac{\partial F_1(\theta_i, \delta_i)}{\partial \theta}}{\frac{\partial F_1(\theta_i, \delta_i)}{\partial \theta} \frac{\partial F_2(\delta_i, \phi_i)}{\partial \delta} \frac{\partial F_3(\phi_i, \theta_i)}{\partial \phi} + \frac{\partial F_1(\theta_i, \delta_i)}{\partial \delta} \frac{\partial F_2(\delta_i, \phi_i)}{\partial \phi} \frac{\partial F_3(\phi_i, \theta_i)}{\partial \theta}}
\end{aligned} \tag{2.19}$$

$$\begin{aligned}
& \Delta \phi_i \\
= & \phi_{i+1} - \phi_i \\
= & \frac{\begin{vmatrix} \frac{\partial F_1(\theta_i, \delta_i)}{\partial \theta} & \frac{\partial F_1(\theta_i, \delta_i)}{\partial \delta} & -F_1(\theta_i, \delta_i) \\ 0 & \frac{\partial F_2(\delta_i, \phi_i)}{\partial \delta} & -F_2(\delta_i, \phi_i) \\ \frac{\partial F_3(\phi_i, \theta_i)}{\partial \theta} & 0 & -F_3(\phi_i, \theta_i) \end{vmatrix}}{D} \\
= & \frac{-F_3(\phi_i, \theta_i) \frac{\partial F_1(\theta_i, \delta_i)}{\partial \theta} \frac{\partial F_2(\delta_i, \phi_i)}{\partial \delta} - F_2(\delta_i, \phi_i) \frac{\partial F_3(\phi_i, \theta_i)}{\partial \theta} \frac{\partial F_1(\theta_i, \delta_i)}{\partial \delta} + F_1(\theta_i, \delta_i) \frac{\partial F_3(\phi_i, \theta_i)}{\partial \theta} \frac{\partial F_2(\delta_i, \phi_i)}{\partial \delta}}{\frac{\partial F_1(\theta_i, \delta_i)}{\partial \theta} \frac{\partial F_2(\delta_i, \phi_i)}{\partial \delta} \frac{\partial F_3(\phi_i, \theta_i)}{\partial \phi} + \frac{\partial F_1(\theta_i, \delta_i)}{\partial \delta} \frac{\partial F_2(\delta_i, \phi_i)}{\partial \phi} \frac{\partial F_3(\phi_i, \theta_i)}{\partial \theta}}
\end{aligned} \tag{2.20}$$

The recursive formulus yields

$$\begin{cases} \theta_{i+1} = \theta_i + \Delta\theta_i \\ \delta_{i+1} = \delta_i + \Delta\delta_i \\ \phi_{i+1} = \phi_i + \Delta\phi_i \end{cases} \quad (2.21)$$

If initial points  $\theta_0$  ,  $\delta_0$  ,  $\phi_0$  are given,  $\theta$  ,  $\delta$  ,  $\phi$  can be computed by recursive operations.

## §2-5 Forward Kinematics

Applying Eq (2.11) to the forward kinematic analysis of the hexglider manipulator, a system of equation with respect to the attitude angles  $\theta$  ,  $\delta$  , and  $\phi$  can be obtained

$$\begin{cases} F^*(\theta, \delta, f_1, g_1, r_1, r_2) = 0 \\ F^*(\delta, \phi, f_2, g_2, r_2, r_3) = 0 \\ F^*(\phi, \delta, f_3, g_3, r_3, r_1) = 0 \end{cases} \quad (2.22)$$

As shown in Figure 2.5, the coordinates of ball joint U1, U2, U3 on the upper plate can be computed with the solved attitude angles  $\theta$  ,  $\delta$  , and  $\phi$

$$U1 = Trans(BR, \sqrt{3}BR - f_1, 0) \cdot Rot(y, -\theta) \begin{bmatrix} 0 \\ 0 \\ r_1 \end{bmatrix} \quad (2.23)$$

$$U2 = Rot(z, 120^\circ) \cdot Trans(BR, \sqrt{3}BR - f_2, 0) \cdot Rot(y, -\delta) \begin{bmatrix} 0 \\ 0 \\ r_2 \end{bmatrix} \quad (2.24)$$

$$U3 = Rot(z, 240^\circ) \cdot Trans(BR, \sqrt{3}BR - f_3, 0) \cdot Rot(y, -\phi) \begin{bmatrix} 0 \\ 0 \\ r_3 \end{bmatrix} \quad (2.25)$$

Substituting the coordinates of ball joints U1, U2, U3 into Eq.(2.26), the coordinates of the center of the end-effector  $p_x$ ,  $p_y$ , and  $p_z$  can be obtained as follows

$$\begin{bmatrix} p_x \\ p_y \\ p_z \end{bmatrix} = (U1 + U2 + U3) / 3 - \begin{bmatrix} 0 \\ 0 \\ IH \end{bmatrix} \quad (2.26)$$

The Euler rotation matrix Eq.(2.27) denotes a set of unit base vectors of the coordinate system describing the pose of the end-effector

$$\begin{aligned} & RPY(\gamma, \beta, \alpha) \\ &= Rot(z, \gamma) \cdot Rot(y, \beta) \cdot Rot(x, \alpha) \\ &= \begin{bmatrix} \cos\gamma \cos\beta & \cos\gamma \sin\beta \sin\alpha - \sin\gamma \cos\alpha & \cos\gamma \sin\beta \cos\alpha + \sin\gamma \sin\alpha \\ \sin\gamma \cos\beta & \sin\gamma \sin\beta \sin\alpha + \cos\gamma \cos\alpha & \sin\gamma \sin\beta \cos\alpha - \cos\gamma \sin\alpha \\ -\sin\beta & \cos\beta \sin\alpha & \cos\beta \cos\alpha \end{bmatrix} \\ &= \begin{bmatrix} u_x & v_x & w_x \\ u_y & v_y & w_y \\ u_z & v_z & w_z \end{bmatrix} \end{aligned} \quad (2.27)$$

As a result, the positions of ball joints U1, U2, and U3 with respect to the coordinates of the center of the end-effector  $p_x$ ,  $p_y$ , and  $p_z$ , the radius of the tangent circle of the equilateral-triangle  $Q_1 Q_2 Q_3$ , UR, and the unit pose vectors of the end-effector  $u_x$ ,  $u_y$ ,  $u_z$  can be derived as Eq.(2.28), Eq.(2.29), and



Eq.(2.30).

$$U1 = \begin{bmatrix} p_x + UR \cdot u_x \\ p_y + UR \cdot u_y \\ p_z + UR \cdot u_z \end{bmatrix} \quad (2.28)$$

$$U2 = \begin{bmatrix} p_x - \frac{1}{2}UR \cdot u_x + \frac{\sqrt{3}}{2}UR \cdot v_x \\ p_y - \frac{1}{2}UR \cdot u_y + \frac{\sqrt{3}}{2}UR \cdot v_y \\ p_z - \frac{1}{2}UR \cdot u_z + \frac{\sqrt{3}}{2}UR \cdot v_z \end{bmatrix} \quad (2.29)$$

$$U3 = \begin{bmatrix} p_x - \frac{1}{2}UR \cdot u_x - \frac{\sqrt{3}}{2}UR \cdot v_x \\ p_y - \frac{1}{2}UR \cdot u_y - \frac{\sqrt{3}}{2}UR \cdot v_y \\ p_z - \frac{1}{2}UR \cdot u_z - \frac{\sqrt{3}}{2}UR \cdot v_z \end{bmatrix} \quad (2.30)$$

Rewrite Eq.(2.28), Eq.(2.29), and Eq.(2.30),  $\gamma$ ,  $\beta$ , and  $\alpha$  can be computed from Eq.(2.31), Eq.(2.32), and Eq.(2.33).

$$\gamma = \text{Tan}^{-1}\left(\frac{U1_y - p_y}{U1_x - p_x}\right) \quad (2.31)$$

$$\beta = \text{Sin}^{-1}\left(\frac{U1_z - p_z}{UR}\right) \quad (2.32)$$

$$\alpha = \text{Sin}^{-1}\left(\frac{U2_z - U3_z}{\sqrt{3}UR \cdot \text{Cos}\beta}\right) \quad (2.33)$$

## Chapter 3

### Modeling of Motion Errors

#### §3.1 Introduction

The SP-120 is a six degree of freedom parallel manipulator which is presently the one used for modeling the false circular cotour of motion errors resulting from the individual error sources of the manipulator. With the results of simplified forward kinematics, the position deviations generated by geometric error sources, especially assembly errors, are derived mathematically in this chapter. Simutaneously, the parameter errors relating to the geometric error sources are described as well.



#### §3.2 Error Descriptions

All of the errors are coupled in any parallel manipulator. Therefore, the total possible errors can be summed and expressed in terms of the Taylor expansion as follows:

$$\begin{aligned} & \text{Total error} \\ &= E(x, c_1, c_2, \dots, c_m) \\ &= c_1 E_1(x) + c_2 E_2(x) + \dots + c_m E_m(x) \end{aligned} \tag{3.1}$$

Geometric resources of motional deviations, including translate and angular ones, resulting from the manufacturing or assembly of guideways and linkages

are classified and modeled with the analytical results of the kinematics in the thesis.

As shown in Fig 3.1, the geometric resources of motional deviations under investigation can be classified and described as follows.

(1) Linkage length error

The length errors of the six linkages due to the the manufacturing tolerances may affect the pose accuracy of the manipulator.

(2) Slider positioning error

The positioning errors of the six sliders S1 to S6 are usually generated from the controller, and they might exist at the initialized command data.

(3) Assembly errors for the guideways

Three guideways are assembled on the stationary plate. Three ball joints are mounted on the mobile plate as well. The improper positions of fixing guideways or ball joints may lead to assembly errors. The assembly errors can be categorized into the following items:

1. Guideway translation error ; In Figure 3.2 (a), the guideway is translated a positional error along the X , Y , or Z axis.
2. Guideway rotation error (I) ; In Figure 3.2 (b), the guideway is rotated an angular error by the center of the guide way on XY or YZ plane.

3. Guideway rotation error (II) ; In Figure 3.2 (c), the guideway is rotated an angular error about the center of the tri-angle, consist of three guideways and fixed on the base plate, on XY plane.

The angular and positional deviations of the end-effector in the machine coordinate system are defined. There are thirty three deviations in a hexglider manipulator. In the following, We begin to model the above deviations with the analytical results of the kinematics.

### §3.3 Error Modeling

#### (1) Translation errors of the guide way

##### a) Translation error along X-axis

[Type I]

In Figure 3.3, a translation error  $\lambda_{XI}$  along the X-axis of the right guideway is added. The position of the ball joint U2 is taken from Eq.(2.10), and the true position of the ball joint U1 becomes

$$U1' = Trans(\lambda_{XI}, 0, 0) \cdot U1 \quad (3.2)$$

After simplifying the equation, the distance between U1' and U2 yields

$$b^2 = f^2 + g^2 + q^2 + r^2 - fg - \sqrt{3}gr\sin\theta - \sqrt{3}fq\sin\delta + qr\sin\theta\sin\delta - 2qr\cos\theta\cos\delta + \lambda_{XI}(\sqrt{3}g - q\sin\delta - 2r\sin\theta) \quad (3.3)$$

Eq (3.3) can be expressed as

$$F_1 = f^2 + g^2 + q^2 + r^2 - b^2 - fg - \sqrt{3}gr\sin \theta - \sqrt{3}fq\sin \delta + qr\sin \theta\sin \delta - 2qr\cos \theta\cos \delta + \lambda_{XII} (\sqrt{3}g - q\sin \delta - 2r\sin \theta)$$
(3.4)

[Type II]

Figure 3.4 shows a translation error  $\lambda_{XII}$  along the X-axis of the left guideway is added. We can get the position of the ball joint U1 from Eq.(2.9) and derive the true position of the ball joint U2

$$U_2' = Trans \left( -\frac{\lambda_{XII}}{2}, \frac{\sqrt{3}\lambda_{XII}}{2}, 0 \right) \cdot U_2$$
(3.5)

The distance between U1 and U2' yields

$$b^2 = f^2 + g^2 + q^2 + r^2 - fg - \sqrt{3}gr\sin \theta - \sqrt{3}fq\sin \delta + qr\sin \theta\sin \delta - 2qr\cos \theta\cos \delta + \lambda_{XII} (\sqrt{3}f - r\sin \theta - 2q\sin \delta)$$
(3.6)

Eq (3.5) can be expressed as

$$F_2 = f^2 + g^2 + q^2 + r^2 - b^2 - fg - \sqrt{3}gr\sin \theta - \sqrt{3}fq\sin \delta + qr\sin \theta\sin \delta - 2qr\cos \theta\cos \delta + \lambda_{XII} (\sqrt{3}f - r\sin \theta - 2q\sin \delta)$$
(3.7)

*b) Translation error along Y-axis*

[Type I]

In Figure 3.5, a translation error  $\lambda_{YI}$  along the Y-axis of the right guideway is added. The position of the ball joint U2 remains the same and is taken from Eq.(2.10). The true position of the ball joint U1 becomes

$$U_1' = Trans (0, \lambda_{YI}, 0) \cdot U_1$$
(3.8)

Simplify the distance **b** between U1' and U2 and obtain

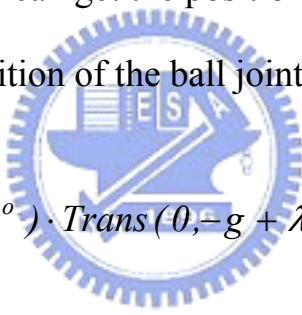
$$b^2 = f^2 + g^2 + q^2 + r^2 - fg - \sqrt{3}gr\sin\theta - \sqrt{3}fq\sin\delta + qr\sin\theta\sin\delta - 2qr\cos\theta\cos\delta + \lambda_{YI}(g - 2f - \sqrt{3}q\sin\delta) \quad (3.9)$$

Eq (3.9) can be expressed as

$$F_3 = f^2 + g^2 + q^2 + r^2 - b^2 - fg - \sqrt{3}gr\sin\theta - \sqrt{3}fq\sin\delta + qr\sin\theta\sin\delta - 2qr\cos\theta\cos\delta + \lambda_{YI}(g - 2f - \sqrt{3}q\sin\delta) \quad (3.10)$$

[Type II]

Figure 3.6 shows a translation error  $\lambda_{YII}$  along the Y-axis of the left guideway is added .We can get the position of the ball joint U1 form Eq.(2.9) and derive the true position of the ball joint U2



$$U2' = Rot(z, -60^\circ) \cdot Trans(0, -g + \lambda_{YII}, 0) \cdot Rot(y, \delta) \begin{bmatrix} 0 \\ 0 \\ q \end{bmatrix} \quad (3.11)$$

Simplify the distance **b** between U1 and U2' and obtain

$$b^2 = f^2 + g^2 + q^2 + r^2 - fg - \sqrt{3}gr\sin\theta - \sqrt{3}fq\sin\delta + qr\sin\theta\sin\delta - 2qr\cos\theta\cos\delta + \lambda_{YII}(f - 2g - \sqrt{3}r\sin\theta) \quad (3.12)$$

Eq (3.12) can be expressed as

$$F_4 = f^2 + g^2 + q^2 + r^2 - b^2 - fg - \sqrt{3}gr\sin\theta - \sqrt{3}fq\sin\delta + qr\sin\theta\sin\delta - 2qr\cos\theta\cos\delta + \lambda_{YII}(f - 2g - \sqrt{3}r\sin\theta) \quad (3.13)$$

c) Translation error along Z-axis

[Type I]

In Figure 3.7, a translation error  $\lambda_{ZI}$  along the Z-axis of the right guideway is added. The position of the ball joint U2 remains the same and is taken from Eq.(2.10). The true position of the ball joint U1 becomes

$$U1' = Trans(0,0, \lambda_{ZI}) \cdot U1 \quad (3.14)$$

Simplify the distance **b** between U1' and U2 and obtain

$$b^2 = f^2 + g^2 + q^2 + r^2 - fg - \sqrt{3}gr\sin\theta - \sqrt{3}fq\sin\delta + qr\sin\theta\sin\delta - 2qr\cos\theta\cos\delta + 2\lambda_{ZI}(r\cos\theta - q\cos\delta) \quad (3.15)$$

Eq (3.15) can be expressed as

$$F_5 = f^2 + g^2 + q^2 + r^2 - b^2 - fg - \sqrt{3}gr\sin\theta - \sqrt{3}fq\sin\delta + qr\sin\theta\sin\delta - 2qr\cos\theta\cos\delta + 2\lambda_{ZI}(r\cos\theta - q\cos\delta) \quad (3.16)$$

[Type II]

Figure 3.8 shows a translation error  $\lambda_{ZII}$  along the Z-axis of the left guideway is added .We can get the position of the ball joint U1 form eq.(2.9) and derive the true position of the ball joint U2

$$U2' = Trans(0,0, \lambda_{ZII}) \cdot U2 \quad (3.17)$$

The distance between U1 and U2' yields

$$b^2 = f^2 + g^2 + q^2 + r^2 - fg - \sqrt{3}gr\sin\theta - \sqrt{3}fq\sin\delta + qr\sin\theta\sin\delta - 2qr\cos\theta\cos\delta - 2\lambda_{ZII}(r\cos\theta - q\cos\delta) \quad (3.18)$$

Eq (3.18) can be expressed as

$$F_6 = f^2 + g^2 + q^2 + r^2 - b^2 - fg - \sqrt{3}gr\sin\theta - \sqrt{3}fq\sin\delta + qr\sin\theta\sin\delta - 2qr\cos\theta\cos\delta - 2\lambda_{zII}(r\cos\theta - q\cos\delta) \quad (3.19)$$

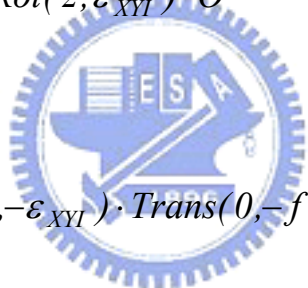
## (2) Rotation errors of the Guide way

### a) Rotatation error on XY plane

[Type I]

In Figure 3.9, a rotatation error  $\varepsilon_{XYI}$  on the XY-plane is added to the right guideway. The position of the ball joint U2 remains the same and is taken from Eq.(2.10). The true position of the ball joint U1 becomes

$$O = \begin{bmatrix} 0 \\ BR\sqrt{3} \\ 0 \end{bmatrix}, \quad O' = Rot(z, \varepsilon_{XYI}) \cdot O$$

$$U1' = (O' - O) + Rot(z, -\varepsilon_{XYI}) \cdot Trans(0, -f, 0) \cdot Rot(y, -\theta) \begin{bmatrix} 0 \\ 0 \\ r \end{bmatrix} \quad (3.20)$$


Simplify the distance **b** between U1' and U2 and obtain

$$b^2 = f^2 + g^2 + q^2 + r^2 - b^2 - fg - \sqrt{3}gr\sin\theta - \sqrt{3}fq\sin\delta + qr\sin\theta\sin\delta - 2qr\cos\theta\cos\delta + \varepsilon_{XYI}[-\sqrt{3}fg - 3 \cdot BR \cdot f + (2\sqrt{3} \cdot BR + g)r\sin\theta + (\sqrt{3} \cdot BR + f)q\sin\delta + \sqrt{3}qr\sin\theta\sin\delta] \quad (3.21)$$

Eq (3.21) can be expressed as

$$F_7 = f^2 + g^2 + q^2 + r^2 - b^2 - fg - \sqrt{3}gr\sin\theta - \sqrt{3}fq\sin\delta + qr\sin\theta\sin\delta - 2qr\cos\theta\cos\delta + \varepsilon_{XYI}[-\sqrt{3}fg - 3 \cdot BR \cdot f + (2\sqrt{3} \cdot BR + g)r\sin\theta + (\sqrt{3} \cdot BR + f)q\sin\delta + \sqrt{3}qr\sin\theta\sin\delta] \quad (3.22)$$

[Type II]

Figure 3.10 shows a rotatation error  $\varepsilon_{XYII}$  on the XY-plane is added to



the guideway B2B3. We can get the position of the ball joint U1 from Eq.(2.9) and derive the true position of the ball joint U2

$$O = \begin{bmatrix} \frac{3BR}{2} \\ BR\sqrt{3} \\ \frac{2}{0} \end{bmatrix}, \quad O' = Rot(z, -\varepsilon_{XYII}) \cdot O$$

$$U2' = (O' - O) + Rot1(z, -60^\circ - \varepsilon_{XYII}) \cdot Trans(0, -g, 0) \cdot Rot(y, \delta) \begin{bmatrix} 0 \\ 0 \\ q \end{bmatrix} \quad (3.23)$$

Simplify the distance b between U1 and U2' and obtain

$$b^2 = f^2 + g^2 + q^2 + r^2 - fg - \sqrt{3}gr\sin\theta - \sqrt{3}fq\sin\delta + qr\sin\theta\sin\delta - 2qr\cos\theta\cos\delta + \varepsilon_{XYII}[-\sqrt{3}fg + 3 \cdot BR \cdot f + (\sqrt{3} \cdot BR - g)r\sin\theta + (2\sqrt{3} \cdot BR - f)q\sin\delta - \sqrt{3}qr\sin\theta\sin\delta] \quad (3.24)$$

Eq (3.24) can be expressed as

$$F_8 = f^2 + g^2 + q^2 + r^2 - b^2 - fg - \sqrt{3}gr\sin\theta - \sqrt{3}fq\sin\delta + qr\sin\theta\sin\delta - 2qr\cos\theta\cos\delta + \varepsilon_{XYII}[-\sqrt{3}fg + 3 \cdot BR \cdot f + (\sqrt{3} \cdot BR - g)r\sin\theta + (2\sqrt{3} \cdot BR - f)q\sin\delta - \sqrt{3}qr\sin\theta\sin\delta] \quad (3.25)$$

### b) Rotatation error on YZ plane

[Type I]

In Figure 3.11, a rotatation error  $\varepsilon_{YZI}$  on the YZ-plane is added to the right guideway. The position of the ball joint U2 remains the same and is taken from Eq.(2.10). The true position of the ball joint U1 becomes

$$O = \begin{bmatrix} 0 \\ BR\sqrt{3} \\ 0 \end{bmatrix}, \quad O' = Rot(x, \varepsilon_{YZI}) \cdot O$$

$$U1' = (O' - O) + Rot(x, -\varepsilon_{YZI}) \cdot Trans(0, -f, 0) \cdot Rot(y, -\theta) \begin{bmatrix} 0 \\ 0 \\ r \end{bmatrix} \quad (3.26)$$

Simplify the distance **b** between U1' and U2 and obtain

$$b^2 = f^2 + g^2 + q^2 + r^2 - fg - \sqrt{3}gr\sin\theta - \sqrt{3}fq\sin\delta + qr\sin\theta\sin\delta - 2qr\cos\theta\cos\delta + \varepsilon_{YZI}[-\sqrt{3}fg + gr\sin\theta + fq\sin\delta + 2\sqrt{3} \cdot BR \cdot (r - q)\cos\delta + \sqrt{3}qr\sin\theta\sin\delta] \quad (3.27)$$

Eq (3.27) can be expressed as

$$F_9 = f^2 + g^2 + q^2 + r^2 - b^2 - fg - \sqrt{3}gr\sin\theta - \sqrt{3}fq\sin\delta + qr\sin\theta\sin\delta - 2qr\cos\theta\cos\delta + \varepsilon_{YZI}[-\sqrt{3}fg + gr\sin\theta + fq\sin\delta + 2\sqrt{3} \cdot BR \cdot (r - q)\cos\delta + \sqrt{3}qr\sin\theta\sin\delta] \quad (3.28)$$

[Type II]

Figure 3.12 shows a rotation error  $\varepsilon_{YZII}$  on the YZ-plane is added to the left guideway. We can get the position of the ball joint U1 from Eq.(2.9) and derive the true position of the ball joint U2

$$O = \begin{bmatrix} 0 \\ BR\sqrt{3} \\ 0 \end{bmatrix}, \quad O' = Rot(x, -\varepsilon_{YZII}) \cdot O$$

$$U2' = (O' - O) + Rot(z, -60^\circ) \cdot Rot(x, -\varepsilon_{YZII}) \cdot Trans(0, -g, 0) \cdot Rot(y, \delta) \begin{bmatrix} 0 \\ 0 \\ q \end{bmatrix} \quad (3.29)$$

Simplify the distance b between U1 and U2' and obtain

$$b^2 = f^2 + g^2 + q^2 + r^2 - fg - \sqrt{3}gr\sin\theta - \sqrt{3}fq\sin\delta + qr\sin\theta\sin\delta - 2qr\cos\theta\cos\delta + \varepsilon_{YZH}[-2(g + \sqrt{3} \cdot BR)r\cos\theta + (f + 2\sqrt{3} \cdot BR)q\cos\delta + \sqrt{3}qr\sin\theta\sin\delta] \quad (3.30)$$

Eq (3.30) can be expressed as

$$F_{10} = f^2 + g^2 + q^2 + r^2 - b^2 - fg - \sqrt{3}gr\sin\theta - \sqrt{3}fq\sin\delta + qr\sin\theta\sin\delta - 2qr\cos\theta\cos\delta + \varepsilon_{YZH}[-2(g + \sqrt{3} \cdot BR)r\cos\theta + (f + 2\sqrt{3} \cdot BR)q\cos\delta + \sqrt{3}qr\sin\theta\sin\delta] \quad (3.31)$$

The deviations due to rotating the guide way on the XZ plane will not be derived because the joint of the RSSR mechanism is free.

(c) *Rotation error about the center of the base on XY plane*

[Type I]

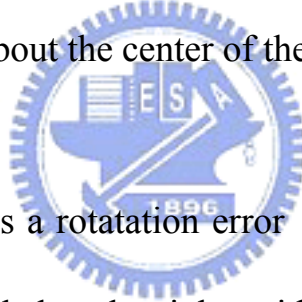


Figure 3.13 shows a rotation error  $\varepsilon_{OI}$  about the center of the base on the XY-plane is added to the right guideway. We can get the position of the ball joint U2 from Eq.(2.9) and derive the true position of the ball joint U1

$$O = \begin{bmatrix} BR \\ BR\sqrt{3} \\ 0 \end{bmatrix}$$

$$O' = Rot(z, \varepsilon_{OI}) \cdot O$$

$$U1 = (O - O') + Rot(z, \varepsilon_{OI}) \cdot Trans(0, -f, 0) \cdot Rot(y, -\theta) \begin{bmatrix} 0 \\ 0 \\ r \end{bmatrix} \quad (3.32)$$

Simplify the distance between U1' and U2 and obtain

$$\begin{aligned}
 b^2 = & f^2 + g^2 + q^2 + r^2 - fg - \sqrt{3}gr\sin\theta - \sqrt{3}fq\sin\delta + qr\sin\theta\sin\delta - 2qr\cos\theta\cos\delta \\
 & + \varepsilon_{OI}[\sqrt{3}fg - 2 \cdot BR \cdot (f + g) + (2\sqrt{3} \cdot BR - g)r\sin\theta + (2\sqrt{3} \cdot BR - f)q\sin\delta - \sqrt{3}qr\sin\theta\sin\delta]
 \end{aligned} \quad (3.33)$$

Eq (3.33) can be expressed as

$$\begin{aligned}
 F_{II} = & f^2 + g^2 + q^2 + r^2 - b^2 - fg - \sqrt{3}gr\sin\theta - \sqrt{3}fq\sin\delta + qr\sin\theta\sin\delta - 2qr\cos\theta\cos\delta \\
 & + \varepsilon_{OI}[\sqrt{3}fg - 2 \cdot BR \cdot (f + g) + (2\sqrt{3} \cdot BR - g)r\sin\theta + (2\sqrt{3} \cdot BR - f)q\sin\delta - \sqrt{3}qr\sin\theta\sin\delta]
 \end{aligned} \quad (3.34)$$

[Type II]

Figure 3.14 shows a rotation error  $\varepsilon_{OII}$  about the center of the base on the XY-plane is added to the left guideway. We can get the position of the ball joint U1 from Eq.(2.9) and derive the true position of the ball joint U2

$$OI = \begin{bmatrix} BR \\ BR\sqrt{3} \\ 0 \end{bmatrix}, \quad OI' = Rot(z, \varepsilon_{OII}) \cdot OI$$

$$U2' = (OI - OI') + Rot(z, -60^\circ + \varepsilon_{OII}) \cdot Trans(0, -g, 0) \cdot Rot(y, \delta) \begin{bmatrix} 0 \\ 0 \\ q \end{bmatrix} \quad (3.35)$$

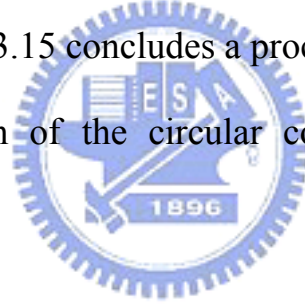
Simplify the distance between U1 and U2' and obtain

$$\begin{aligned}
 b^2 = & f^2 + g^2 + q^2 + r^2 - fg - \sqrt{3}gr\sin\theta - \sqrt{3}fq\sin\delta + qr\sin\theta\sin\delta - 2qr\cos\theta\cos\delta \\
 & - \varepsilon_{OII}[\sqrt{3}fg - 2 \cdot BR \cdot (f + g) + (2\sqrt{3} \cdot BR - g)r\sin\theta + (2\sqrt{3} \cdot BR - f)q\sin\delta - \sqrt{3}qr\sin\theta\sin\delta]
 \end{aligned} \quad (3.36)$$

Eq (3.36) can be expressed as

$$\begin{aligned}
F_{12} = & f^2 + g^2 + q^2 + r^2 - b^2 - fg - \sqrt{3}gr\sin\theta - \sqrt{3}fq\sin\delta + qr\sin\theta\sin\delta - 2qr\cos\theta\cos\delta \\
& - \varepsilon_{0II}[\sqrt{3}fg - 2 \cdot BR \cdot (f + g) + (2\sqrt{3} \cdot BR - g)r\sin\theta + (2\sqrt{3} \cdot BR - f)q\sin\delta - \sqrt{3}qr\sin\theta\sin\delta]
\end{aligned}
\tag{3.37}$$

Table 3.1 summarizes the kinematic equations relating to a variety of geometric errors for the RSSR mechanism. Systems of equations, retrieved and correlated from the kinematic equations listed in Table 3.1, in terms of the attitude angles  $\theta$ ,  $\delta$ , and  $\phi$  for any error condition discussed above can be obtained as shown in Table 3.2. Due to the geometric error, the new coordinates of the ball joints U1', U2', U3' on the upper mobile plate can be computed with the solved attitude angles  $\theta$ ,  $\delta$ ,  $\phi$  of a corresponding system of equations listed in Table 3.2. Figure 3.15 concludes a procedure of modeling the deviations along the radial direction of the circular contour under the effects of the geometric errors.



### §3.4 Error diagnosis

The simulation plots of the radial deviations varying along the circular contour under the interaction of the error sources discussed in the previous section are presented as Figure 3.16 ~ Figure 3.20. These data are used as the reference data for identifying the deviations. In practice, a combination of these individual errors may lead to the incorrect pose of the end effector. For improving the position and orientation accuracy of the end effector, diagnosing the parameter errors relating to the faulty manufacture and assembly can be

beneficial to either revising the incorrect parts or adjusting the improper assembly of the mechanism, or compensating errors in the controller.

At first, the correlated parameter errors (deviations) in mathematic models are defined and the radial circular motion errors due to various kinds of individual error sources are derived respectively. Then the measured data, the composite error, based on the DBB test is obtained experimentally and applied to the estimation of error parameters with the least square method, which will be mentioned in chapter 5. Referring to these error parameters, deviations of the end-effector of the six degree-of-freedom manipulator may be compensated in the controller repeatedly so that the position and orientation precision of it can be promoted effectively.



## Chapter 4

### Measurement of Motion Errors

#### §4-1 Double Ball Bar Measurement Device

The double ball bar (DBB) consists of a precision linear transducer (LVDT), whose accuracy is  $\pm 1$  micrometer over a measurement range of 2 mm with 1 micrometer resolution, an extension bar, a magnetic central mount with a central ball, and a magnetic tool cup, as shown in Figure 4.1. A ball joint is attached to the end of the transducer and magnetically coupled to the magnetic tool cup located somewhere on the auxiliary fixture. The transducer provides electrical signals converted electrically into a form which can be read by the computer software and hence captured and analyzed. The extension bar has a three points supported ball socket at the free end and form a ball joint with the central ball on the base plate. A permanent magnet is integrated in the socket so that the extension bar and the central ball can be held together by magnetic force. The length of the extension bar determines the radius of the test circular. The central ball is fixed on the magnetic central mount with a thread after the central mount is not aligned until the ball joint is directly underneath the tool cup.

## §4-2 Experimental Planning

The technique of the double ball bar (DBB) is applied to measuring the contouring error of the desired six degree-of-freedom manipulator, as shown in Figure 4.2. The magnetic tool cup is hold on the auxiliary fixture. The maganetic central mount is mounted on the center of the mobile plate of the manipulator. The ballbar transducer is connected with the extension bar. After the DBB being setup, the ball of the free end of the transducer will be coupled with the magnetic tool cup, and the socket of the extension bar and the central ball will be held together by the magnetic force.

The planned experiment, as shown in Figure 4.3, includes two parts : the first part is the setup of the DBB system, and the second one is the data capture of the circular contour. The procedures of the setup and data capture of the DBB test are illustrated in Figure 4.4. The main steps are summarized as follows:

1. Locate the center position of the simulation mobile plate, and then place the central amount with the central ball on it.
2. Fix the magnetic tool cup on the auxiliary fixture properly. Move the mobile plate toward the the magnetic tool cup. After the tool cup and central ball are coupled and aligned, lock the central ball tightly, and then reset the position of the mobile plate.
3. Move the mobile plate downward with an distance of approximate 5 cm away from the tool cup, and then move it to the start point of the circular tracking.



4. Attach the ballbar transducer with extension bar to the tool cup and the central ball.
5. Start the operation of the data capture with moving the mobile plate along a circular contour clockwise, and then perform it counterclockwise.
6. Acquire the datum and analyze them.

Before doing the experiment, two things which have got to be ready are as follows:

1. Unlike conventional machine tools, it is not convenient for the SP-120 to have no spindle for holding the tool cup. Therefore, it is necessary to design and fabricate an auxiliary fixture before setting up the DBB system, as shown in Figure 4.5.
2. For capturing data, the first step needed is to write a program for moving the mobile plate along a test path of circular contour. The test path is shown in Figure 4.6. When data is captured dynamically, the program may drive the ballbar through the angular overshoot and data capture arcs.

#### §4-3 Experimental Results

Figure 4.7 shows the test of the double ball bar for the target hexglider manipulator. The central ball on the mobile plate is fixed at the position of the center. The radius of the circular contour is 100mm. The feed speed is set to

753.98 mm/min for the circular motion.

Figure 4.8 demonstrates the polar plot of the test result.



## Chapter 5

### Least Squares Estimation

#### §5-1 Error Estimation

Let  $x$  be the slider positions,  $x \in \mathfrak{R}^6$ , all  $p$  of the kinematic parameters of the parallel manipulator can be contained in the vector  $\beta \in \mathfrak{R}^p$ , and the reading from the ball bar,  $y \in \mathfrak{R}^T$ . Since the ball bar is a passive joint, the end effector pose  $\rho$  will be determined by the kinematic parameters and the slider positions,  $\rho = \text{forkin}(x, \beta)$ . Once the pose is determined, the length of the ball bar is fixed through the inverse kinematics by  $y = \text{invkin}(\rho, \beta)$ . These relationships can be combined to give

$$y = \text{invkin}(\text{forkin}(x, \beta), \beta) = f(x, \beta) \quad (5.1)$$

The function  $f$  is a numerical function that combines the inverse and forward kinematics of the parallel manipulator. The relationship given by the above equation holds for the actual values  $y, x$ , and  $\beta$ . In reality, these values are corrupted by unknown errors. Therefore, Eq. (5.1) is more accurately stated as

$$\bar{y} + \tilde{y} = f(\bar{x} + \tilde{x}, \bar{\beta} + \tilde{\beta}) \quad (5.2)$$

where the notation stands for nominal values in the case of  $\beta$ , slider positions of  $x$ , the ball bar reading of  $y$ , and the tilda notation represents small

deviations. Over a series of  $i = 1 \dots n$  poses, Eq. (5.2) becomes

$$\bar{y}_i + \tilde{y}_i = f(\bar{x}_i + \tilde{x}_i, \bar{\beta} + \tilde{\beta}) \quad (5.3)$$

The goal of the diagnosis is the way to find a combination of deviations (errors) that satisfies Eq. (5.3). The diagnosis should not just find any combination of deviations, but it should find the “best” combination. By formulating the diagnosis as a least square minimization, deviations will be estimated. In this chapter, it is the major work we will concentrate on.

## §5-2 Least Square Method

Consider a system of linear equations :

$$\mathbf{Ax} = \mathbf{b}$$

Where  $\mathbf{A} \in \mathbb{R}^{m \times n}$ ,  $\mathbf{b} \in \mathbb{R}^m$ ,  $m \geq n$ , and  $\text{rank } \mathbf{A} = n$ . Note that the number of unknowns,  $n$ , is no longer than the number of equations,  $m$ . If  $\mathbf{b}$  does not belong to the range of  $\mathbf{A}$ ; that is, if  $\mathbf{b} \notin \mathcal{R}(\mathbf{A})$ , then this system of equations is said to be inconsistent or overdetermined. In such case, there is no solution to the above set of equations. Our goal is to find the vector (or vectors)  $\mathbf{x}$  minimizing  $\|\mathbf{Ax} - \mathbf{b}\|^2$

Let  $\mathbf{x}^*$  be a vector that minimizes  $\|\mathbf{Ax} - \mathbf{b}\|$ ; that is, for all  $\mathbf{x} \in \mathbb{R}^m$ ,

$$\|\mathbf{Ax} - \mathbf{b}\|^2 \geq \|\mathbf{Ax}^* - \mathbf{b}\|^2$$

We refer to the vector  $\mathbf{x}^*$  as a least-squares solution to  $\mathbf{Ax} = \mathbf{b}$ . In the case where  $\mathbf{Ax} = \mathbf{b}$  has a solution, then the solution is a least-squares solution. Otherwise, a least-squares solution minimizes the norm of the difference

between the left- and right-hand sides of the equation  $\mathbf{Ax} = \mathbf{b}$ . The unique vector  $\mathbf{x}^*$  that minimizes  $\|\mathbf{Ax} - \mathbf{b}\|^2$  is given by the solution to the equation

$$\mathbf{A}^T \mathbf{Ax} = \mathbf{A}^T \mathbf{b} \quad (5.4)$$

that is,

$$\mathbf{x}^* = (\mathbf{A}^T \mathbf{A})^{-1} \mathbf{A}^T \mathbf{b} \quad (5.5)$$

In view of considering a fitting function  $\hat{y}$  with a form of the linear combination of several known functions  $f_i$ , the fitting function  $\hat{y}$  can be written as follow :

$$\hat{y} = f(x, c_1, c_2, \dots, c_m) = c_1 f_1(x) + c_2 f_2(x) + \dots + c_m f_m(x) \quad (5.6)$$

where the dependent variable  $\hat{y}$  is linear with respect to coefficients  $c_1, c_2, \dots, c_m$ .

Let  $\mathbf{x}$  is a set of independent variables  $x_1, x_2, x_3, \dots, x_n$ , and  $\hat{\mathbf{y}}$  is a set of corresponding dependent variables  $\hat{y}_1, \hat{y}_2, \hat{y}_3, \dots, \hat{y}_n$ . Meanwhile,  $\mathbf{y}$  is the set of datum  $y_1, y_2, y_3, \dots, y_n$  obtained from the experiment. Consequently, the residuals  $r_i$  can be expressed as :

$$\left\{ \begin{array}{l} \sum_{k=1}^m c_k f(x_1) - y_1 = r_1 \\ \sum_{k=1}^m c_k f(x_2) - y_1 = r_2 \\ \dots\dots\dots \\ \sum_{k=1}^m c_k f(x_n) - y_n = r_n \end{array} \right. \quad (5.7)$$


For the sake of minimizing the sum of the squares of the residuals, Eq (5.7) should be satisfied.

$$\sum_{i=1}^n \sum_{k=1}^m r_i \frac{\partial r_i}{\partial c_k} = 0 \quad (5.8)$$

Since

$$\frac{\partial r_i}{\partial c_k} = f_k, \quad k=1,2,3,\dots,m \quad (5.9)$$

Equation (5.8) can be formulated in a matrix form of linear algebraic equations in terms of m undetermined coefficient as follows:

$$\begin{bmatrix} \sum [f_1(x_i)]^2 & \sum [f_1(x_i) \cdot f_2(x_i)] & \cdots & \sum [f_1(x_i) \cdot f_m(x_i)] \\ \sum [f_2(x_i) \cdot f_1(x_i)] & \sum [f_2(x_i)]^2 & \cdots & \sum [f_2(x_i) \cdot f_m(x_i)] \\ \cdot & \cdot & \cdots & \cdot \\ \sum [f_m(x_i) \cdot f_1(x_i)] & \sum [f_m(x_i) \cdot f_2(x_i)] & \cdots & \sum [f_m(x_i)]^2 \end{bmatrix} \begin{bmatrix} c_1 \\ c_2 \\ \cdot \\ c_m \end{bmatrix} = \begin{bmatrix} \sum f_1(x_i) \cdot y_1 \\ \sum f_2(x_i) \cdot y_2 \\ \cdot \\ \sum f_m(x_i) \cdot y_m \end{bmatrix} \quad (5.10)$$


### §5-3 Simulation and Diagnosis

The computer program based on the model we have developed in previous sections simulates a variety of contouring error conditions. These simulation results presented in polar plots are shown in Fig.3.16~Fig.3.20. A phenomena observed in the simulation results reveals that the error contour rotates  $120^\circ$  as the guide way rotates  $60^\circ$  in any error condition we have discussed before. The experimental data based on DBB test are shown in Fig.4.8. as well.

The simulation of the diagnosis using the data generating from the synthesis of theoretical error contours is illustrated as follows. A set of values of parameter errors may be given at first to generate the corresponding contouring errors  $\Delta L_i$  and these contouring errors can be summed to generate a synthetic contouring error. Then we estimate the values of these parameter errors of the synthetic contouring error inversely by means of the least square technique. In comparison with the given values and the identified ones of these parameter errors, we can judge that the estimation (diagnosis) can be judged to be valid or not.

The matrix A is prepared using the reference data corresponding to each deviation as shown in Figure 3.16 ~ Figure 3.20. So far as the diagnosis is concerned, the error model and the measurement strategy should be properly designed to yield a nonsingular matrix  $A^T A$  such that the identified parameters are completely observable. As the solutions of altitude angles  $\theta$ ,  $\delta$ ,  $\phi$  are obtained through the Newton recursive formula and the circular contouring error  $\Delta L_i$  is computed with  $\theta$ ,  $\delta$ , and  $\phi$ , the contouring error term  $\Delta L_i$  will be expressed with numerical forms instead of polynomial forms. Without exact solutions, it is not easy to judge what variables or functions are related to each contouring error  $\Delta L_i$  and whether there exist the relationship of linear independent among all of them. The error estimation begins with the sorting and merging of parameter errors into independent parameters. In the following

practical simulations for diagnosis, we set the guideway B3B1 as the reference one without errors and obtain results as follows:

- (1) In case of taking five geometric errors, including three linkage length errors and two guideway translation errors to execute the error estimation, It can be seen that the identified values of the five motion errors are corresponding to the given ones (shown as Table 5.1).
- (2) In case of taking six geometric errors, including three linkage errors and three guideway translation errors to execute the error estimation, we can find that a part of the identified values of the six motion errors are not corresponding to the given values (shown as Table 5.2).
- (3) In case of taking four geometric errors, including four linkage length errors, we can find that a part of the identified values of the four motion errors are not corresponding to the given values (shown as Table 5.3).
- (4) In case of taking six geometric errors, including three linkage length errors, two guideway translation errors, and a guideway rotating error to execute the error estimation, It can be seen that the identified values of the six motion errors are corresponding to the given ones (shown as Table 5.4).
- (5) In case of taking seven geometric errors, including three linkage errors, two guideway translation errors, and two guideway rotation errors to execute the error estimation, we can find that the identified values of the seven motion errors are corresponding to the given values (shown as Table 5.5).



(6) In case of taking eight (or nine) motion errors, including three linkage length errors, two guideway translation errors, and three (or four) guideway rotation errors to execute the error estimation, we can find that a part of the identified values of the nine motion errors are not corresponding to the given values (shown as Table 5.6 ~ Table 5.7).

As a result, we can identify seven geometric errors, including three linkage length errors, two guideway translation errors, and two guideway rotation errors. The simulation result of the error estimation with data based on DBB test for the manipulator SP-120 is shown as Table 5.8.



## Chapter 6

### Conclusion

In the study, the error modeling based on the numerical method has been performed to analyze the parameter errors corresponding to geometric errors for the hexglider manipulator. We use the Newton-Raphson method to reduce the complexity of the nonlinear equations properly by means of transferring them into linear equations. Then, the least-square technique has been applied to evaluating the coefficients with regard to the linear combination of the modeling errors in order to diagnose the geometric errors resulting in motional deviations.

As for the concrete implement and verification of the error modeling and diagnosis, a computer-aided analysis program has been developed for estimating parameter errors based on the circular contour error measurement using the kinematical double ball bar. The developed software has been applied to a practical case of the hexglider manipulator.

In spite that we can identify geometric errors and make an attempt to approximate the testing curve of a true hexglider manipulator based on the double ball bar test, however, there are still a few error sources, except for geometric errors, existing at a hexglider manipulator and left to be identified for improving the accuracy of a hexglider manipulator. Therefore, it is worthwhile

to make everlasting efforts on exploring the issue in the future.

## References

- [1] Hiromu Nakazawa, 1994, Principles of Precision Engineering, Oxford University press Inc., New York
- [2] 陳金聖, 1993, ”利用雙球桿量測發展數值工具機之誤差判斷與補償技術”, 國立交通大學機械所碩士論文
- [3] Renishaw Ballbar User Guide , Renishaw Co., Ltd.
- [4] ISO 230-1 : Test code for machine tools-Part I : Geometric accuracy of machines operating under no-load or finishing conditions (1996).
- [5] J. Mou., M.A. Donmez , and S. Centikunt, 1995, Adaptive error correction method using feature-based analysis techniques for machine performance improvement, Part I and Part II, ASME, Journal of Engineering for Industry , Vol.14, pp362-369
- [6] Bryan, J.A., 1982, A Simple Method for Testing Measuring Machine and Machine Tools, Precision Engineering, Vol.4, No.2, pp61-69
- [7] Knapp, W., 1983, Test of the Three Dimensional Uncertainty of Machine Tools and Measuring Machines and Its Relationship to the Machine Errors, Annals of the CIRP, Vol.32, pp459-464
- [8] Kunzmann, H., Waldele, F., and Bundesanstalt, P.T., 1983, On Testing Coordinate Measuring Machines (CMM) with Kinematic Reference Standards, Annals of the CIRP, Vol.32, pp465-468

- [9]Kakino, Y., Ihara, Y., and Nakatsu. Y., 1987, The Measurement of Motion Errors of NC Machine Tools and Diagnosis of Their Origins By Using Telescoping Magnetic Ball Bar Method, Annals of the CIRP, Vol.36, pp377-383
- [10]S. L. Jeng , W. H. Chieng , and A. C. Lee, 1996, Modeling and Diagnosis of Motion Error of Multi-Axis Machines Using a Ball Bar Test, ASME Journal of Dynamic System , Measurement , and Control, Vol.118, pp531-539
- [11]M. Tsutsumi, A.Satio, 2003, Identification and compensation of deviations particular to 5-axis machining center, Int.J. of Machine Tools & Manufacture, Vol.43, pp771-780
- [12]D. Stewart, 1965, A platform with six degrees of freedom, in Proc. Inst, Mech. Engr. (London), vol.180, no.15, p.p.371-386
- [13]K.M.Lee and D.K.Shah, 1988, Kinematic analysis of a three-degrees-of-reedom in-parallel actuated manipulator, Journal of Robotics Automation, vol. 4, no. 3, p.p.354-356
- [14]K. Cleary and T.Brooks, 1993, Kinematic analysis of a novel 6-DOF parallel actuated manipulator, Proceedings of IEEE International Conference on Robotics and Automation, p.p.708-713
- [15]P. Nanea, K. J. Waldron, and V. Murthy, 1990, Direct kinematic solution of a stewart platform, Journal of Robotics Automation, vol. 6, no. 6, p.p.371-386

- [16]Husty. M.L., 1994, An algorithm for solving the direct kinematic of Stewart-Gough-type platform, Research report TR-CIM-94-7, CIM, McGill University, Montreal, Canada
- [17]C. W. Wampler and A.P. Morgan, 1990, Numerical continuation methods for solving polynomial systems arising in kinematics, ASME J Mech Des, vol. 112, p.p.59-68
- [18]C. Innocenti and V.Parenti-Castelli, 1993, Forward kinematics of the general 6-6 fully parallel mechanism : An exhaustive numerical approach via mono-dimensional-search algorithm, ASME J Mech Des, vol. 115, p.p.227-282
- [19]J. Wang and O. Masory, 1993, On the accuracy of a Stewart platform-Part I The effect of manufacturing tolerances, Proceedings IEEE International Conference on Robotics and Automation.1,p.p.114-120
- [20]T. Ropponen and T. Arai, 1995, Accuracy analysis of a ModifiedSteward platform manipulator, Proceedings IEEE International Conference on Robotics and Automation, p.p.521- 525
- [21]A.J. Patel and K.F. Ehmann, 1997, Volumetric error analysis of a modified Stewart platform-based machine tool, Annals of the CIRP, 46(1), p.p. 287-290
- [22]J.W. Zhao, K.C.Fan. T.H.Chang and Z.Li, 2002, Error analysis of a Serial-Parallel type machine tool, Advanced manufacturing technology, p.p. 174-179

- [23]H. Zhuang, Z.S.Roth, 1993, Method for kinematic calibration of Steward Platform, Journal of Robotic System 10 (3), pp391-405
- [24]C.A.Wampler, J.M.Hollerbach, T.Arai, 1995, An implicit Ilo method for kinematic calibration and its application to closed-chain mechanisms, IEEE Transaction on Robotics and Automation II (5), pp710-724
- [25]H.Zhuang, L.Liu, 1996, Self-calibration of a class of parallel manipulator, Proceedings of the IEEE International Conference on Robotics and Automation II (5), pp994-999
- [26]A. J. Patel, K. F. Ehmann, 2002, Calibration of a hexapod machine tool using a redundant leg, Int.J. of Machine Tools & Manufacture. Vol.42,pp1151-1170
- [27]Y. J. Chiu, M . H. Perng, 2003, Self-calibration of a general hexapod manipulator using cylinder constraints, Int.J. of Machine Tools & Manufacture. Vol.43, pp1051-1066